Quantitative Insight into Morphology Evolution of Thin PPV/PCBM Composite Films upon Thermal Treatment

Hanfang Zhong,[†,‡] Xiaoniu Yang,*[,†,§,#] Bert deWith,[†,§] and Joachim Loos*[,†,§,⊥]

Laboratory of Materials and Interface Chemistry, Eindhoven University of Technology, PO Box 513, NL-5600 MB Eindhoven, The Netherlands; School of Chemistry and Chemical Technology, Shanghai Jiaotong University, 200240 Shanghai, P. R. China; Dutch Polymer Institute, PO Box 902, NL-5600 AX Eindhoven, The Netherlands; and Laboratory of Polymer Technology, Eindhoven University of Technology, PO Box 513, NL-5600 MB Eindhoven, The Netherlands

Received September 25, 2005; Revised Manuscript Received November 7, 2005

ABSTRACT: Atomic force microscopy (AFM) is used to study the morphology evolution upon thermal treatment of a thin composite film typically used for polymer solar cells application. This film consists of poly[2-methoxy-5-(3′,7′-dimethyloctyloxy)-1,4-phenylenevinylene] (MDMO−PPV) and 1-(3-methoxycarbonyl)propyl-1-phenyl-[6,6]-methanofullerene (PCBM) with 80 wt % of PCBM in the composite. AFM topographic images clearly demonstrate that PCBM crystal clusters grow up out of the film, and the areas surrounding the crystals become thinner due to the depletion of PCBM material, which causes the phase separation in the composite film upon annealing. Volume quantification analysis on these sequential AFM topographic images in-situ recorded during annealing shows that the volumes of both PCBM crystals and depletion zones are significantly increased during the initial annealing times, followed by a stable period indicating the occurrence of equilibrium state. The different morphology evolution kinetics between the depletion zones and PCBM crystals is mostly due to the asynchronism between the move out of PCBM from its original position and collapse down of the film wherein. The global equilibrium state is finally achieved as most of the PCBM in the whole film has been depleted for crystal growth.

Introduction

Polymer solar cells[1] are attracting more and more attention[2−4] from both academic and industrial communities for their multifold advantages including dramatically decreased price potentially, roll-to-roll production, flexibility, light weight of the product, and so on, compared to the traditional photovoltaic (PV) technology. Polymer solar cells now are mostly based on the electron donor and acceptor approach,[5,6] in which donor and acceptor constitutes are brought together within the photoactive layer to form a heterojunction to fulfill energy conversion. Because the typical exciton diffusion length in conjugated polymers is limited to ∼10 nm,[7−9] the donor and acceptor constitutes should form nanoscale interpenetrating networks within the whole photoactive layer to ensure efficient dissociation of the excitons and collection of the free charge carriers afterward. The challenge for morphology control is to organize the donor and acceptor components toward such an objective that their interface area is maximized, while typical dimensions of phase separation are within the exciton diffusion range and continuous, preferably short, pathways for transport of charge carriers to the electrodes are ensured. Having all the above-mentioned advantages, bulk heterojunction[10,11] is the currently the most promising architecture for photoactive layer in polymer solar cells based on the donor−acceptor approach.

The thin-film deposition technique must be used to prepare the photoactive layer for fabrication of a polymer solar cell device. Spin-coating is currently one of the most extensively used techniques from solution-based technology.[12−14] Spin-coating provides a simple and successful way to prepare thin films having homogeneous morphology within a relatively large area. However, the high solvent evaporation rate during its process probably suppresses phase separation, even for a blend that typically would give large-scale phase separation via a more equilibrium preparation method.[15] Hence, thin films prepared via spin-coating are mostly not in their equilibrium state, and likely there is a strong thermodynamic driving force for the samples to reorganize toward the stable equilibrium state. This process will be accelerated at elevated temperatures.[15−18] For polymer solar cell devices, the morphological reorganization within the photoactive layer with time or temperature during either on-shelf period or in operation may seriously affect the performance and long-term stability of the device.[18−20]

In a viewpoint from device performance, i.e., power conversion efficiency, one of the most successful electron donor and acceptor material pairs for polymer solar cells is the MDMO−PPV/PCBM composite.[12,21−23] The bulk-heterojunction solar cell devices with power conversion efficiencies of 2.5%[12,23] under simulated solar light have been achieved in this composite. The morphology evolution of MDMO−PPV/PCBM composite film upon thermal annealing at different temperatures[15] with different PCBM ratios[15] in the composite film or under different spatial-confined environments[16] has been studied mainly by using transmission electron microscopy (TEM). The results show brighter areas surrounding PCBM single crystals possibly due to the depletion of PCBM material for crystal growth for both free-standing and substrate-supported films. In this work, we focus on the detailed morphology evolution, particularly on the PCBM single crystals and corresponding depletion zones by using in-situ atomic force microscopy (AFM) investigations. Afterward, quantitative volume analysis will be applied to characterize the kinetics of PCBM crystallization and formation

† Laboratory of Materials and Interface Chemistry, Eindhoven University of Technology.
‡ Shanghai Jiaotong University.
§ Dutch Polymer Institute.
⊥ Laboratory of Polymer Technology, Eindhoven University of Technology.
Current address: State Key Laboratory of Polymer Physics and Chemistry, Changchun Institute of Applied Chemistry, Chinese Academy of Sciences, Changchun 130022, P. R. China.
* Corresponding authors: E-mail xnyang@ciac.jl.cn or j.loos@tue.nl.

10.1021/ma0520803 CCC: $33.50
Published on Web 12/09/2005

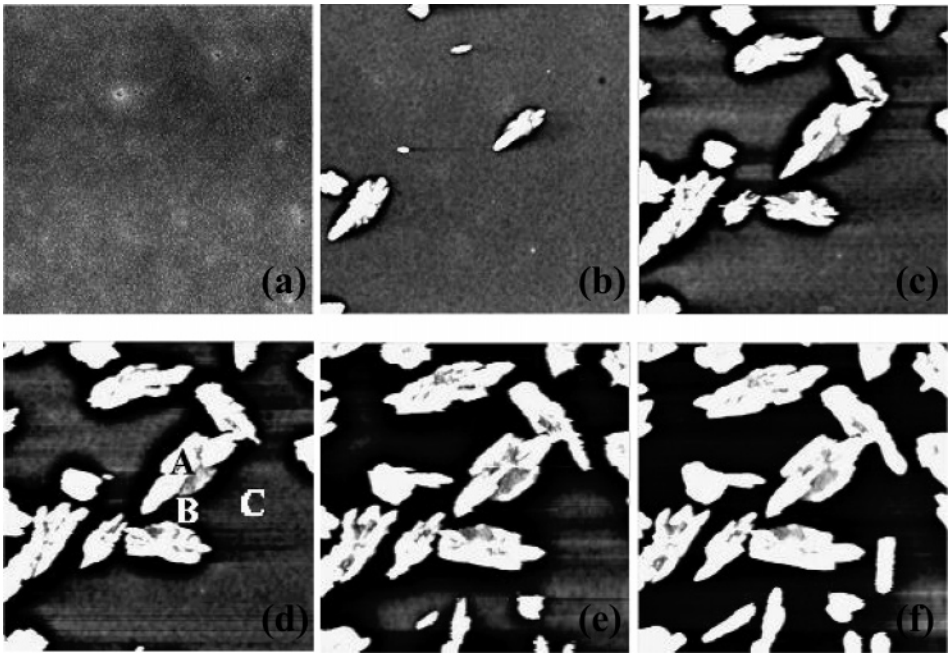

Figure 1. AFM topography images of MDMO−PPV/PCBM composite films (MDMO−PPV:PCBM = 1:4 by weight) in-situ recorded upon annealing at 130 °C for (a) pristine film, (b) 12 min, (c) 22 min, (d) 27 min, (e) 38 min, and (f) 73 min. Scan size: $15 \times 15\ \mu m^2$; height range (from peak to valley): 200 nm. The letters A, B, and C marked in (d) represent the region of the location where the PCBM nucleates and the crystal growths, the depletion zone that is formed due to moving out of PCBM material for the crystal growth, and the unchanged composite film still consists both MDMO−PPV and PCBM, respectively, as described in the text.

of depletion zones. A scheme is proposed finally based on this analysis to describe the detailed morphology evolution of the composite film upon thermal annealing. We eventually intend to find a way to control and stabilize the designed morphology of the photovoltaic layer for polymer solar cells by using phase separation kinetics of thin polymer/molecule composite film upon additional e.g. thermal annealing treatment.

Experimental Part

Materials. For the present study, 1-(3-methoxycarbonyl)propyl-1-phenyl-[6,6]-methanofullerene (PCBM)[24] was synthesized at the University of Groningen, The Netherlands, poly[2-methoxy-5-(3′,7′-dimethyloctyloxy)-1,4-phenylenevinylene] (MDMO−PPV)[25] was obtained from Philips Research Eindhoven, The Netherlands, and poly(ethylenedioxythiophene)−poly(styrenesulfonate) (PEDOT:PSS) was purchased from Bayer AG, Germany.

Sample Preparation. Fresh microscope glass cover slides were used as substrates to prepare the composite film via the spin-coating method. The substrates were first cleaned by acetone and 2-propanol and then treated in a UV-ozone oven for ca. 30 min. MDMO−PPV and PCBM were mixed 1:4 by weight and dissolved in chlorobenzene (CB) and continuously stirred in the dark overnight to form a solution with concentration of 10 mg mL^{-1} for PCBM in the solution. Subsequently, an ∼75 nm thick layer of PEDOT:PSS was spin-coated from an aqueous dispersion under ambient conditions on the cleaned substrate aforementioned. Finally, an ∼80 nm thick composite layer of MDMO−PPV and PCBM was spin-coated on top of the PEDOT:PSS layer.

Atomic Force Microscopy (AFM). A solver P47H atomic force microscope (NT-MDT Co., Moscow, Russia) operated in intermittent-contact mode was used to measure height and phase images with NT-MDT NSG01S cantilevers (force constant is typically 5.5 N m^{-1}) under ambient conditions. The height of AFM has been calibrated using a 25 nm height standard grating produced by NT-MDT Co., Moscow, Russia. The integrated high-temperature heating stage was employed to acquire in-situ topography images while annealing. The temperature stability of the hot stage is controlled within 0.1 °C.

Results and Discussion

To get three-dimensional information on the morphology evolution of the thin composite film on the substrate, AFM operated in intermittent-contact mode is used to acquire topography images during the annealing process. Figure 1 shows a series of AFM topographic images of MDMO−PPV/PCBM composite films in-situ recorded upon annealing at 130 °C for different times. For the pristine film before any thermal treatment (as shown in Figure 1a), a homogeneous morphology within a relatively large area is observed at the scanning resolution we used. Actually, the fresh composite film is composed of PCBM-rich domains with average size of 80 nm distributed in the relatively PCBM-poor MDMO−PPV/PCBM matrix. For the whole composite film, PCBM is condensed as nanocrystal adopting various crystallographic orientations.[15,27]

Upon annealing, PCBM single crystals grow up gradually with annealing time and stick out of the film plane (as shown in Figure 1b−f). Notably, in these AFM topography images, the bright domains are PCBM single crystals (marked as A in Figure 1d), and the dark areas (depletion zones, marked as B in Figure 1d) initially surrounding the PCBM crystals reflect thinner regions of the film, being composed of almost pure MDMP−PPV (i.e., depleted from PCBM). To clearly monitor the evolution of both the PCBM crystals and the depletion zones with time during annealing, a set of cross-sectional profiles across a PCBM single crystal and the surrounding depletion zone are shown in Figure 2. After a PCBM single crystal sticks out from the composite film, the growth continues in both lateral and perpendicular directions. The depletion zone around becomes broader and deeper as annealing goes on. However, simply to compare these topography images, we are not able to judge whether there is a difference in growth kinetics between the PCBM crystals and the depletion zones around, which reflects how the PCBM molecules diffuse within the composite film and finally contribute to the formation of PCBM single crystals. To acquire exact growth kinetics for both the PCBM

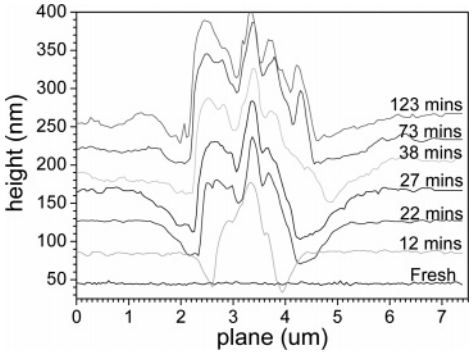

Figure 2. Cross-sectional profiles across a PCBM single-crystal cluster and the depletion zone around in-situ recorded during annealing at 130 °C for the given times. The curves have been shifted along *Y*-axis to give a clearer demonstration.

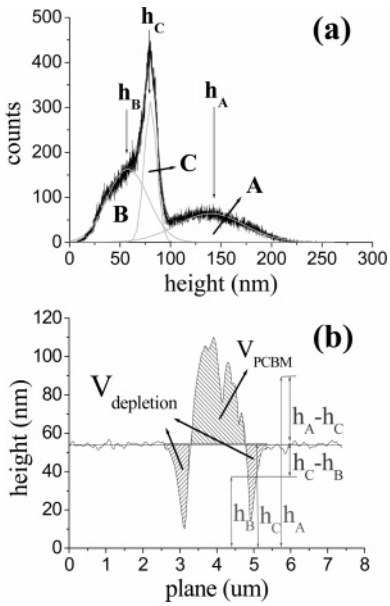

Figure 3. (a) Height distribution histogram obtained from AFM topography image of Figure 1d, which is resolved into three parts A, B, and C. Part A denotes the area of the PCBM single crystals, B the area of the depletion zones surrounding the PCBM crystals, and C the area of the original film plane. h_A, h_B, and h_C represent the peak positions of Gaussian fitted curves corresponding to the PCBM single crystals, the depletion zones, and the original film plane, respectively. (b) Schematic representation of cross-sectional profile across a PCBM crystal and depletion zone around. The values of h_A, h_B, and h_C are obtained from (a).

crystals and the depletion zones, volume quantification calculations were applied to topographic images from the composite film annealed for different times similar to the areas shown in Figure 1 but with scan size of 100 × 100 μm, from which the detailed volume evolution of either the PCBM single crystals or depletion zones could be resolved. Since the calculations are carried out based on quite large areas of the composite films, the results make statistical sense.

In an AFM topography image, the main information that each pixel actually carried is a relative height value. For an image with the dimensions of 512 × 512 pixels, correspondingly, there are 262 144 height values with the image. If a specific resolution of the height value is given, a curve can be plot by the total number of pixels which have the height value within the given resolution vs this height value. This plot actually gives a height distribution histogram for the whole topography image. Figure 3a shows the histogram of height counts from the image of Figure 1d. Three dominant peaks can be resolved from this histogram by using Gaussian distribution fitting with good fitting quality of $R^2 = 0.9847$.

As shown in Figure 3a, in a typical height distribution histogram obtained from a topography image the three Gaussian distribution fitted curves can be assigned to the PCBM single crystals (A), depletion zones surrounding the PCBM crystals (B), and the original film surface (C). During the posttreatment of each topography image, the smallest height value measured within the whole film is set to zero, and the height values of the other pixels are recalculated with respect to this reference to produce a relative height value for each pixel measured. Therefore, as shown in the cross-sectional profile of Figure 3b, h_A, h_B, and h_C, the height values associated with the three peaks corresponding to the regions A, B, and C as shown in Figure 1d, represent the relative average height of the depletion zones, of the original film surface plane, and of the PCBM crystals, respectively. Hence, $h_A - h_C$ denotes the average height of the PCBM crystals and $h_C - h_B$ the average depth of depletion zones with respect to the original film surface plane. Thus, the volumes of depletion zones and the PCBM crystals can be determined by using eqs 1 and 2, respectively.

$$V_{\text{depletion}} = [P_B(h_C - h_B)]\frac{A_{\text{pix}}}{l_h} \quad (1)$$

$$V_{\text{PCBM}} = [P_A(h_A - h_C)]\frac{A_{\text{pix}}}{l_h} \quad (2)$$

where $V_{\text{depletion}}$ denotes the volume of depletion zones, V_{PCBM} the volume of PCBM crystals, P_A the pixel count of the PCBM single crystals, P_B the pixel count of the depletion zones, A_{pix} the truly physical area size one pixel occupies (for example, scan size of 1000 nm × 1000 nm/(512 pixel × 512 pixel) = 3.81 nm^2/pixel), and l_h the height step, i.e., resolution of the height parameter during the AFM measurement (0.07 nm in our case). We would like to note that the volume of the depletion zones refers to the surface volume of depletion zones with respect to the original film surface plane, and the volume of PCBM crystals denotes the surface volume of crystal clusters out of the original film plane, as shown in Figure 3b. To monitor the volume relationship between depletion zones $V_{\text{depletion}}$ and PCBM single crystals V_{PCBM} during annealing process, we introduce the parameter R (eq 3).

$$R = \frac{V_{\text{depletion}}}{V_{\text{PCBM}}} = \frac{P_B(h_C - h_B)}{P_A(h_A - h_C)} \quad (3)$$

Kontturi et al. have already discussed the error of volume quantification in detail with respect to mainly the effect of the size of AFM tip.[26] In their case, the average height of sample features on a silicon wafer substrate was about 1 nm, which is much smaller compared with the mean width (20 nm) of those features. Correspondingly, an ~6% average exaggeration factor, which mainly results from the physical size of the AFM tip with a radius of curvature between 5 and 10 nm, contributes to the error of the volume quantification. In our case, both the average depth of depletion zones (10−30 nm) and the average height of the PCBM crystals (40−100 nm) are also much smaller compared to their width (2−5 μm), together with the much more pronounced absolute dimensions of the PCBM crystals and the depletion zones with respect to the radius of curvature of the tips we used, can only minimize the error. However, a maximum error of 6% is still assumed for the error consideration. Moreover, the error of height values caused by the measure-

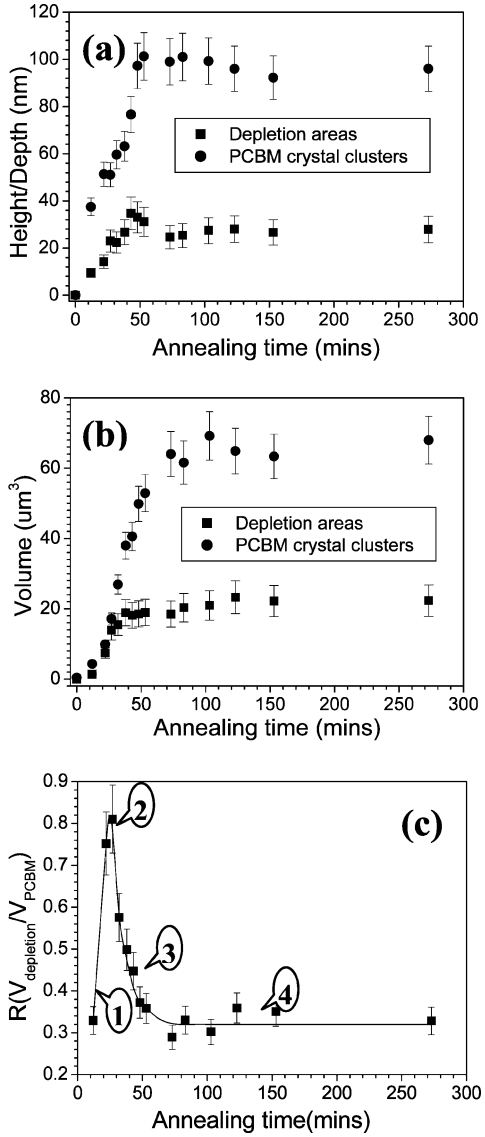

Figure 4. (a) Average depth of the depletion zones and average height of the PCBM crystals vs annealing time. (b) Volume of the depletion zones and the PCBM crystals vs annealing time. (c) Evolution of R (the ratio of $V_{depletion}$ to V_{PCBM}) with annealing time. (The curve is a guide to the eyes; the numeric labels indicate the different periods of morphology evolution upon thermal annealing.)

ments of soft sample material in intermittent-contact mode are within 5−10% after comparing with standard samples. Finally, all fitting quality factors (R^2) using Gaussian distributions are better than 0.97 so that it can be concluded that the total error for volume quantification is within ca. 11−16%.

Figure 4a,b shows the average depth/height and volume values of the depletion zones and PCBM crystals vs annealing time. The average depth of the depletion zones increases significantly for the initial annealing times (from 0 to 43 min), as shown in Figure 4a. The increased depth, together with enlarged lateral dimensions, contributes to the significant volume increase of the depletion zones during the initial annealing period. Later on, both the average depth and volume of the depletion zones keep constant or increase slightly, indicating an equilibrium state being reached. For the PCBM crystals, overall they have the similar height and volume evolution behavior compared with that of the depletion zones; i.e., both the average height and volume increase tremendously at the initial annealing times, followed by almost constant values during the subsequent annealing. However, the annealing time to maximize both the average height and volume of the PCBM crystals is somewhat longer than those of the depletion zones.

With respect to the PCBM crystals, annealing times to reach the maximum value for their average height and volume are asynchronous. The average height reaches its maximum earlier than the volume does as thermal annealing goes on, indicating growth of PCBM crystals is faster in height direction than in lateral direction. This result is consistent with AFM topographic images as shown in Figure 1; the PCBM crystals demonstrate large height values already immediately after their appearing from the composite film.

To reveal volume relationship between depletion zones and PCBM crystals, the parameter R, which is defined as a ratio of the volume of depletion zones to that of the PCBM crystals as given in eq 3, is introduced to quantify the data set obtained during the annealing process. The plot of R as a function of annealing time is shown in Figure 4c. The R value dramatically increased as annealing starts and reaches its maximum at an annealing time of ca. 25 min. Afterward, it rapidly decreases within another 25 min of annealing, and finally it reaches the equilibrium state with constant value until the end of the experiment.

To give detailed descriptions how the depletion zones and PCBM crystals evolve during annealing process, we have divided a typical cross-sectional profile of the composite film in the vicinity of a PCBM crystal into three regions marked as regions A, B, and C (as shown in Figure 5). Region A represents the location where the PCBM nucleates and the crystal growths. Region B represents the depletion zone that is formed due to moving out of PCBM material for the crystal growth. Region C is the unchanged composite film which still consists of both MDMO−PPV and PCBM. The dots represent the PCBM molecules or nanocrystals in the composite. For the initial film, PCBM is condensed as nanocrystalline clusters or molecules homogeneously distributed in the thin composite film in both lateral and perpendicular directions with respect to the film plane. After the first very short annealing time, for instance 12 min in this experiment, the R value becomes ca. 0.3 and rapidly increases to over 0.8 at an annealing time of ca. 25 min, as marked by points 1 and 2, respectively, in Figure 4c. We would like to note that due to the presence of a substrate for the film supporting, the diffusion rate of the PCBM close to the substrate is lower than that on the film surface,[16] which causes the somehow asymmetric PCBM concentration profile in the direction perpendicular to the film plane during thermal annealing.

The reason for this tremendous change of R value within the initial annealing times is probably because of asynchronism between the move out of PCBM from its original position to be incorporated in crystals and the collapse down of the remaining MDMO−PPV matrix. However, because of the certain mechanical stability of the MDMO−PPV matrix, the kinetics of collapse might be delayed compared with the diffusion kinetics of PCBM and thus growth kinetics of the PCBM crystals. At the very initial annealing time, as shown in Figure 5a, the volume amount of film collapsed is smaller compared to that of the diffused PCBM inserted in the crystals. As annealing goes on, more and more PCBM is diffused toward the crystals, which ultimately causes a sudden collapse of large areas of the remaining MDMO−PPV matrix, which contributes to the rapid increased R value for this period (Figure 5b). As annealing time moves on further, the R value rapidly decreases from its maximum (Figure 4c, point 3). This behavior reflects that almost the whole MDMO−PPV matrix film has been

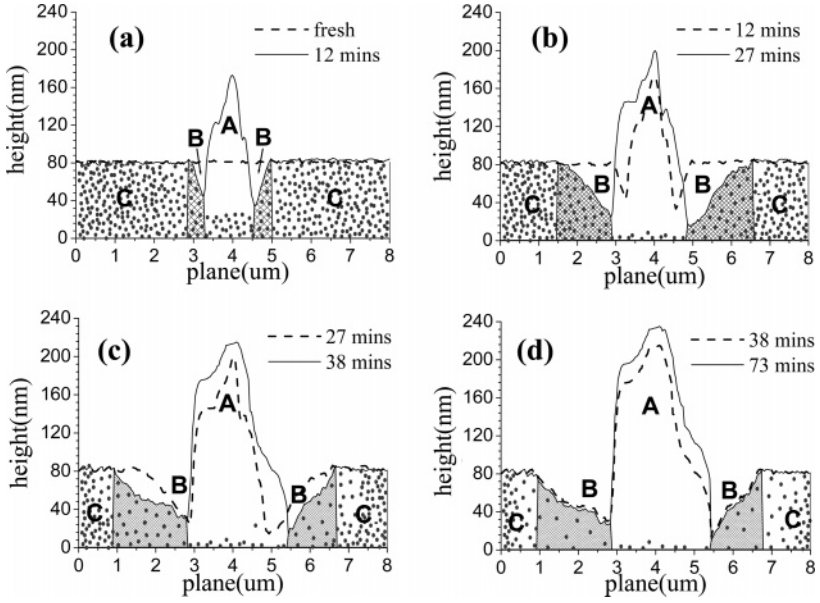

Figure 5. Schematic representations of the detailed morphology evolutions of thin MDMO−PPV/PCBM composite film upon thermal treatment. The dots in the profile represent PCBM molecules/nanocrystals, and density of the dots represents the richness of PCBM; the diamond outlined regions represent the depletion zones after PCBM material moved out for crystal growth, in which the density of diamond outlines represents the richness of MDMO−PPV.

collapsed; however, PCBM diffusion and crystal growth still continue (Figure 5c). Finally, the diffusion rate of PCBM within the whole film decreases, reaching its equilibrium state, as shown in Figure 5d.

The prominent morphology evolution of thin MDMO−PPV/PCBM composite films at elevated temperature is a typical phenomenon observed at various annealing temperatures (even as low as 60 °C for free-standing thin film), with different PCBM ratios in the composite and under various spatial confinements. This morphological change of the composite film is ascribed to the diffusion of PCBM molecules within the MDMO−PPV matrix at elevated temperature and subsequent crystallization of PCBM molecules into large-scale crystals. However, for the high performing polymer solar cell, the phase separation between electron donor and acceptor components should be controlled within a designed range to ensure a large interface for excitons to be dissociated efficiently. Large-scale phase separation enormously reduces the size of this interface area, which causes significantly decreased performance or even leads to failure of the device. Therefore, large phase separation between donor and acceptor components should be prevented during both device fabrication and in operation, particularly at elevated temperature. However, a well-controlled aggregation of both components actually benefits the device performance because it still maintains the large interface between electron donor and acceptor, and at the same time, it provides more continuous pathways for free charge carriers to be transported to the appropriate electrodes, which have been shown to be a key point for improving the performance of polymer solar cell.[28] In viewpoint from this aspect, the phase separation in the thin composite film upon annealing can be utilized to tune the phase dimensions toward a desired length scale for polymer solar cell application. The most important issue that we should take consideration is the conformity of morphology achieved in a real device compared to the designed and required morphology based on the functionality of the device. Therefore, the detailed morphology evolution process and kinetics of phase separation upon thermal annealing in the thin composite film provides indispensable parameters for building up of a morphology control scheme.[29]

Conclusion

In summary, in-situ AFM topography measurements and volume quantification have been used to study the morphology evolution of thin MDMO−PPV/PCBM composite films upon thermal annealing, particularly the crystallization kinetics of the PCBM crystals and the formation kinetics of the depletion zones surrounding these crystals have been revealed quantitatively. Sequential AFM topography images show clearly that PCBM crystals grow up and stick out of film plane and that the areas surrounding the crystals become thinner due to the depletion of PCBM material. For the PCBM crystals, both the average height and volume are significantly increased during the initial annealing times to their maximum values, followed by the periods with almost constant values indicating the approach of the equilibrium states. The annealing time to reach the maximum for the average height of PCBM crystals, however, is shorter than that for the volume, which confirms the crystal growth has priority in height direction than lateral dimensions. With respect to the depletion zones, features of their evolution are similar to that of the PCBM crystals except that the annealing times to the maxima for both average height and volume are shorter than those for PCBM crystals.

The asynchronism of the formation kinetics between the depletion zones and the PCBM crystals is resulted from the delayed film collapse of the remaining MDMO−PPV matrix after PCBM has moved out for crystal growth. The morphology evolution of the composite film ultimately arrives at the equilibrium state as a result of a balanced diffusion of PCBM within the whole composite film after most of the PCBM has been exhausted for the crystal growth.

Acknowledgment. This work is partly supported by the Dutch Polymer Institute (projects DPI #326 and #508). We thank Philips for a generous gift of MDMO−PPV. We thank Dr. Alexander Alexeev for his endeavors in helping us with AFM measurements. H.Z. thanks European Union for financial support through European Union (EU) Asia-Link program ASI/B7-301/98/679-32.

References and Notes

(1) Brabec, C. J.; Sariciftci, N. S.; Hummelen, J. C. *Adv. Funct. Mater.* **2001**, *11*, 15.
(2) Hoppe, H.; Sariciftci, N. S. *J. Mater. Res.* **2004**, *19*, 1924.
(3) Spanggaard, H.; Krebs, F. C. *Sol. Energy Mater. Sol. Cells* **2004**, *83*, 125.
(4) Coakley, K. M.; McGehee, M. D. *Chem. Mater.* **2004**, *16*, 4533.
(5) Tang, C. W. *Appl. Phys. Lett.* **1986**, *48*, 183.
(6) Sariciftci, N. S.; Smilowitz, L.; Heeger, A. J.; Wudl, F. *Science* **1992**, *258*, 1474.
(7) Yoshino, K.; Hong, Y. X.; Muro, K.; Kiyomatsu, S.; Morita, S.; Zakhidov, A. A.; Noguchi, T.; Ohnishi, T. *Jpn. J. Appl. Phys., Part 2* **1993**, *32*, L357.
(8) Halls, J. J. M.; Pichler, K.; Friend, R. H.; Moratti, S. C.; Holmes, A. B. *Appl. Phys. Lett.* **1996**, *68*, 3120.
(9) Haugeneder, A.; Neges, M.; Kallinger, C.; Spirkl, W.; Lemmer, U.; Feldmann, J. *Phys. Rev. B* **1999**, *59*, 15346.
(10) Yu, G.; Gao, J.; Hummelen, J. C.; Wudl, F.; Heeger, A. J. *Science* **1995**, *270*, 1789.
(11) Halls, J. J. M.; Walsh, C. A.; Greenham, N. C.; Marseglia, E. A.; Friend, R. H.; Moratti, S. C.; Holmes, A. B. *Nature* **1995**, *376*, 498.
(12) Shaheen, S. E.; Brabec, C. J.; Sariciftci, N. S.; Padinger, F.; Fromherz, T.; Hummelen, J. C. *Appl. Phys. Lett.* **2001**, *78*, 841.
(13) Halls, J. J. M.; Arias, A. C.; MacKenzie, J. D.; Wu, W. S.; Inbasekaran, M.; Woo, E. P.; Friend, R. H. *Adv. Mater.* **2000**, *12*, 498.
(14) Liu, J.; Shi, Y. J.; Yang, Y. *Adv. Funct. Mater.* **2001**, *11*, 420.
(15) Yang, X. N.; van Duren, J. K. J.; Janssen, R. A. J.; Michels, M. A. J.; Loos, J. *Macromolecules* **2004**, *37*, 2151.
(16) Yang, X. N.; Alexeev, A.; Michels, M. A. J.; Loos, J. *Macromolecules* **2005**, *38*, 4289.
(17) Hoppe, H.; Niggemann, M.; Winder, C.; Kraut, J.; Hiesgen, R.; Hinsch, A.; Meissner, D.; Sariciftci, N. S. *Adv. Funct. Mater.* **2004**, *14*, 1005.
(18) Padinger, F.; Fromherz, T.; Denk, P.; Brabec, C. J.; Zettner, J.; Hierl, T.; Sariciftci, N. S. *Synth. Met.* **2001**, *121*, 1605.
(19) Kroon, J. M.; Wienk, M. M.; Verhees, W. J. H.; Hummelen, J. C. *Thin Solid Films* **2002**, *403*−*204*, 223.
(20) Chirvase, D.; Parisi, J.; Hummelen, J. C.; Dyakonov, V. *Nanotechnology* **2004**, *15*, 1317.
(21) Brabec, C. J.; Shaheen, S. E.; Winder, C.; Sariciftci, N. S.; Denk, P. *Appl. Phys. Lett.* **2002**, *80*, 1288.
(22) van Duren, J. K. J.; Yang, X. N.; Loos, J.; Bulle-Lieuwma, C. W. T.; Sieval, A. B.; Hummelen, J. C.; Janssen, R. A. J. *Adv. Funct. Mater.* **2004**, *14*, 425.
(23) Wienk, M. M.; Kroon, J. M.; Verhees, W. J. H.; Knol, J.; Hummelen, J. C.; van Hal, P. A.; Janssen, R. A. J. *Angew. Chem., Int. Ed.* **2003**, *42*, 3371.
(24) Hummelen, J. C.; Knight, B. W.; LePeq, F.; Wudl, F.; Yao, J.; Wilkins, C. L. *J. Org. Chem.* **1995**, *60*, 532.
(25) Becker, H.; Spreitzer, H.; Kreuder, W.; Kluge, E.; Schenk, H.; Parker, I.; Cao, Y. *Adv. Mater.* **2000**, *12*, 42.
(26) Kontturi, E.; Thune, P. C.; Alexeev, A.; Niemantsverdriet, J. W. *Polymer* **2005**, *46*, 3307.
(27) Yang, X. N.; van Duren, J. K. J.; Rispens, M. T.; Hummelen, J. C.; Michels, M. A. J.; Loos, J. *Adv. Mater.* **2004**, *16*, 802.
(28) Yang, X. N.; Loos, J.; Veenstra, S. C.; Verhees, W. J. H.; Wienk, M. M.; Kroon, J. M.; Michels, M. A. J.; Janssen, R. A. J. *Nano Lett.* **2005**, *5*, 579.
(29) Peumans, P.; Uchida, S.; Forrest, S. R. *Nature* **2003**, *425*, 158.

MA0520803